Ultrafine grinding of mica in organic medium for ink-jet printing process

Naima Boughazif, Fabien Gerschwitz, Julie Bourret, Gisèle Lecomte-Nana, André Lecomte, Martine Lejeune, Vincent Rat, Marguerite Bienia

Powder Technology 442 (2024) 119868

Contents lists available at ScienceDirect

Powder Technology

journal homepage: www.journals.elsevier.com/powder-technology

Ultrafine grinding of mica in organic medium for ink-jet printing process

Naima Boughazif, Fabien Gerschwitz, Julie Bourret, Gisèle Lecomte-Nana, André Lecomte, Martine Lejeune, Vincent Rat, Marguerite Bienia *

Institute for Research on Ceramics (IRCER), CNRS UMR 7315 - Centre Européen de la Céramique - 12, rue Atlantis, 87068, Limoges cedex, France

GRAPHICAL ABSTRACT

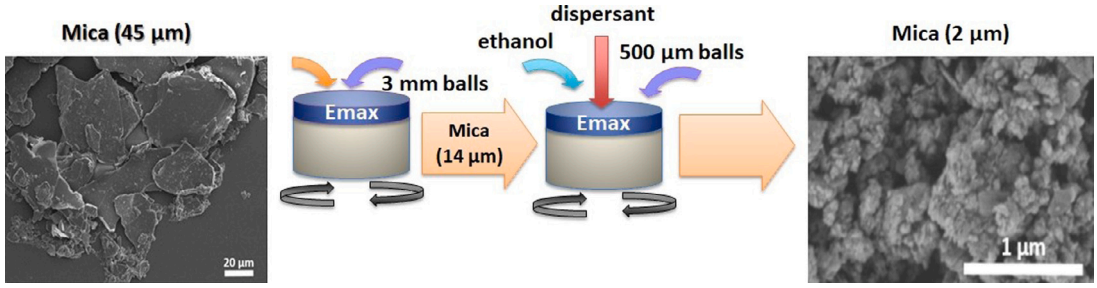

HIGHLIGHTS

- Mica powder is efficiently ground using a new high energy mill (Emax, Retsch).
- Optimal parameters are found to reach a size below 1 µm.
- Structural and morphological properties are conserved after milling.

ARTICLE INFO

Keywords:
Mica
Wet grinding
Dry grinding
High-energy ball milling
Particle size

ABSTRACT

This work investigates the grinding of a mica powder in an organic medium in order to make the particle size compatible with the inkjet process using a high-energy ball mill. A detailed protocol leading to size reduction without altering structural properties of interest of this material has been successfully developed. Two steps are necessary, namely dry grinding and wet grinding in ethanol. The final particle size obtained was D_{90} = 1.9 µm which is very close to the size requirement of the inkjet process related to the printing nozzle diameter (52 µm). The mica morphology in the form of platelets was shown to be conserved by means of scanning electron microscope observations. X-ray diffraction confirmed that the mica did not undergo any change in its crystallographic structure. The decrease in particle size was revealed by the broadening and intensity drop of the diffraction peaks. Thermogravimetric analyses highlighted a shift of dehydroxylation reactions towards lower temperatures, which is also coherent with platelet size reduction.

* Corresponding author.
E-mail address: marguerite.bienia@unilim.fr (M. Bienia).
URL: http://www.ircer.fr/ (M. Bienia).

https://doi.org/10.1016/j.powtec.2024.119868
Received 29 September 2023; Received in revised form 24 November 2023; Accepted 14 May 2024
Available online 17 May 2024

Table 1
Examples of mica grinding from the literature with associated parameters.

Ref	type	Wet/dry	Application	Initial state	Final state	Duration
[11]	knife-mill sonication	both	pearlescent pigment	2 cm	80 μm	10 min
[12]	planetary mill	dry	effect on mica properties	800 μm	60-30 μm	30-360 min
[14]	sonication	wet	effect on mica properties	2 mm	4 μm 450 nm	10 h 100 h
[15]	attritor	wet	effect on mica properties	1–2 mm	–	75 h
[16]	agate mortar	dry	structural change	200 μm	–	100 h
[17]	micro grinder	dry	effect on water release	40–50 μm	4–18 m^2/g	15 min-100 h
[18]	ring-roller mill	both	mill performance	200 μm	100 μm	5–20 s
[19]	rotating knives	wet	effect of grinding medium	1–2 mm	75 m^2/g	50 h
[20]	ball mill	wet	effect of solvent on grinding	1–2 mm	48 m^2/g	12 h

1. Introduction

Among the phyllosilicate family, mica has many industrial applications thanks to its sheet crystallographic structure giving rise to unique physicochemical, electric, mechanical, thermal and mineralogical properties [1–3]. Its application fields include capacitors, plastic fillers, insulators, pigments and aeronautical industry [4]. Previous studies were performed in order to produce 3D components for various applications using ceramic materials by the inkjet process [5,6]. Many applications include fuel cells [7,8] or other electronic components [9, 10]. Given the electrical and thermal properties of mica, it seems a promising candidate for inkjet printing of 2D or 3D components. However, the powder must be of a size compatible with the diameter of the printing nozzles, in order not to obstruct them. Nozzle suppliers recommend using powders for which 90% by volume of the particles (D_{90}) have a diameter fifty times smaller than the opening diameter of the printing nozzles [6]. The opening diameter of the nozzles used in our case is 52 μm, which imposes a D_{90} lower than 1 μm. Generally, micas in their natural state are not as fine (several hundreds of micrometers) [11,12], so grinding is necessary.

Mica grinding is considered as an industrial challenge because of its laminar structure and mechanical properties. Its hardness ranges between 2.8 and 3.2 according to the Mohs scale. A combination of impact, friction and delamination is necessary for size reduction. Moreover, the finer the particles, the more friction is necessary [13], often associated with longer grinding times (10 h for grinding by sonication in [14]). Table 1 summarizes some results from the literature about grinding of mica.

For long dry grinding processes, the decrease in particle size is often associated to a change in structural and physicochemical properties due to the mechanical stresses undergone by the particles, such as alteration of the crystals [21], amorphization and polymorphic transformations [22]. This has been observed for different types of clays as reported by [23–25] for kaolinite, [26] for bentonite, [27] for montmorillonite and [28] for mica (ripidolite). Mica grinding has been performed by various mills such as the knife mill. It allows for particle size reduction down to 100 μm, without destroying or altering the mica platelets because this grinding process minimizes the attrition and impact forces applied to the particles [11]. Studies done by Vdović et al. demonstrated that mica grinding using a high energy planetary mill (Pulverisette 7, Fritsch), leads to a decrease in the particle size and the formation of a polydisperse powder with an irregular particle shape, where large aggregates composed of nanoparticles are formed and where all the structural features typical for clay minerals disappeared [28].

The structural and physico-chemical properties of ground mica particles depend not only on the grinding process used and its parameters (speed, duration, chemical nature and size of grinding balls, etc.), but they also depend on the solvent in case of wet grinding. Wet grinding of mica has been studied in various liquids, such as aqueous media, organic media (methanol and toluene) or alkaline chloride solutions (KCl or LiCl) by Papirer et al. [15,19,20]. They found that grinding in water and methanol preserves the structural properties of mica (muscovite). These authors suggested that this is due to the strong hydrogen bonds in these media. It is known that water molecules on the surface of clays such as muscovite can play the role of a lubricating agent, which can modify the distribution of mechanical forces applied to the mica surface [29]. On the contrary, grinding in toluene destroys the structure, because of the absence of surface charges. The presence of these charges in the aqueous medium prevents particle agglomeration, then hindering the amorphization of the muscovite. They also observed that the presence of species which facilitate the breaking of hydrogen bonds, such as NH_3 in methanol or Li^+ ions in water, destroys the crystalline structure of muscovite during grinding.

Table 2
Chemical and mineral compositions of the mica powder (wt %) according to the supplier.

Chemical	(wt %)	Mineral	(wt %)
SiO_2	48		
Al_2O_3	33	Muscovite	84
K_2O	9.1	Kaolinite	10
MgO	0.8	Quartz	4
Fe_2O_3	2.4	K Feldspar	2

In this work, the feasibility of grinding mica particles towards a size below 1 μm for inkjet printing application is investigated. The aim is to use an efficient way with regards to time and energy consumption in laboratory conditions while retaining the original crystalline structure and morphology, with the least additives possible. To do so, the raw powder was ground using a new type of ball mill for high energy milling (Emax, Retsch) according to the supplier recommendations. The milling parameters have been adjusted to produce the largest ground powder yield. The powder size distribution, morphology and crystal structure were monitored at each step of the grinding process to detect any change induced by the milling.

The material and methods section describes the physico-chemical characteristics of the raw mica powder and the characterization methods used during this work. The adjustment of the grinding steps is presented in the results section. The evolution of structural and physicochemical properties and the impact of grinding on their evolution are then discussed.

2. Materials and methods

2.1. Mica

The mica powder used in this study was purchased from Imerys (France). Its chemical and mineralogical compositions provided by the supplier are reported in Table 2.

It mostly contains muscovite (84 wt %) and a little kaolinite (10 wt %). The laser particle size analysis provided by the supplier shows a particle size distribution with a D_{50} of 20 μm, a D_{90} of 50 μm and a D_{100} of 200 μm. Muscovite belongs to the group of phyllosilicates (layered minerals) having an interlaminar distance of about 1.0 nm [30]. Its TOT elemental layer is formed by an octahedral sheet (O) containing hexacoordinated Al^{3+} ions which is located between two tetrahedral (T) SiO_4 sheets. In the tetrahedral sheet, one Si^{4+} out of four is replaced by

Al^{3+} giving rise to a total negative layer charge. This negative charge is compensated by K^+ cations located between two layers. When such a structure is cleaved, K^+ ions are free and, in the presence of water, are replaced by protons. Kaolinite is also a phyllosilicate but of TO structure (alternating tetrahedral **(T)** and octahedral **(O)** sheets).

Generally, polar materials such as mica are ground in water or ethanol [24]. Ethanol is chosen as the solvent for wet route because of its faster evaporation, which helps collecting the powder after grinding. A steric dispersant (composed of polyether phosphate) was used in small amount (1.5% in weight over the powder) to avoid agglomeration.

2.2. Grinding process

2.2.1. Milling

A high energy ball mill (Emax, Retsch, Germany) was used in this work. It applies both friction and impact forces on the particles [31]. It is equipped with a cooling system in order to reduce heating. The jars volume is 125 mL and they are covered in zirconia. The rotating speed and grinding durations can be selected. In this work, the grinding speed was set at 1700 rpm in order to maximize the effects of frictional and impact forces applied on the particles. This corresponds to 85% of the maximum speed (2000 rpm). After preliminary tests, the duration was set to 20 min. Some empiric rules and recommendations for grinding parameters are found in the literature [32].

1. First, the balls need to be harder than the milled material [19], hence the choice of zirconia (hardness 8–8.5, density 5900 kg/m^3) for both jars and balls. The size of the balls needs to be at least 3 times larger than the size of the particles in order to provide enough energy to break them.
2. The size of the ground particles is expected to be decreased down to around 1/1000 the size of the balls
3. For final sizes smaller than 10 μm, wet grinding is the only option, in order to disperse them to avoid their attraction to each other by electrostatic charges. Theses interactions can be neutralized in a solvent using dispersion techniques.
4. Concerning dry grinding, it is important to fill about 1/3 of the jar with balls, 1/3 with sample material and 1/3 with air to leave enough space for ball movement. For wet grinding, to increase the friction surface required for producing very fine particles, 60% of the jar (in volume) is filled with grinding balls.
5. The jars are successively filled with the grinding balls, then the powder and lastly by the solvent in the case of wet grinding. All volumes are expressed as apparent filling level ratios in the jars (some powder and solvent can fall between the balls). In this work, the nomenclature x-y-z is used, where x, *y* and z correspond respectively to the apparent volume filling of balls, powder and ambient medium (air or ethanol). The choice of the volume of powder is also important. The right amount is needed to have a high probability of particle-grinding body and particle–particle meeting, while giving the medium a moderate viscosity allowing the circulation of the elements in the jar.

Following these recommendations and [33], since the raw mica powder has an initial size up to 200 μm, grinding was done in two steps: (1) dry grinding to reach a size of 10 μm (2) wet grinding in ethanol to decrease the size below 1 μm. Size distribution and other structural and morphological parameters described below were monitored initially and after each grinding step. For the dry step, no additive was used in order not to pollute the system. As previously mentioned, a steric dispersant must however be used for the wet step to limit agglomeration (1.5% w/w_{powder}).

2.2.2. Characterization methods

Particle density was measured by gas pycnometry with an AccuPyc II (Micromeritics) using Helium. Particle size distribution was monitored after each grinding step using laser diffraction analysis using a Mastersizer 3000 (Malvern). The measurements were in ethanol. A small amount from the ground mica powder or suspension was collected from the jar and diluted in ethanol in order to avoid multiple scattering as required by this technique. The suspensions were subjected to sonication for 2 min to break the agglomerates. The size distributions in volume and all relevant characteristic diameters D_{10}, D_{50} and D_{90}, which correspond respectively to the size of 10%, 50% and 90% of the volume of the particles, were obtained. Since some caution should be used with regard to the granulometry analysis which uses Mie's theory for spheres, other relevant physical parameters were measured such as the specific surface area. It was obtained by the BET method on the raw powder and after each grinding step by using 3Flex surface characterization analyzer (Micromeritics). The measurement was carried out after degassing of the powder sample at 90 °C for 30 min then at 250 °C for 2 h.

In order to monitor the morphology of the particles throughout the grinding process, the powders were observed by scanning electron microscope **(SEM)** on a LEO 1530VP (Zeiss). The powders were first dispersed in ethanol and then vibrated by sonotrode for 30 s to break the agglomerates. A drop of suspension was placed on a sample holder (glass slide), and then dried on a heating plate for 3 min at 100 °C. Then, a layer of a few nanometers of platinum was deposited on the surface of the samples using a sputter coater (AGAR B7340), to ensure good flow of excess electrons and avoid the accumulation of charges on the surface of the sample.

To check for any structural changes, X-ray diffraction analyses of the raw and ground mica powders were performed by using a D8 Advance Da Vinci diffractometer (Bruker). The diffraction patterns were collected at room temperature using Cu Kα radiation and variable slits. The scanning angle 2θ ranges from 5 to 90° with a step resolution of 0.02° leading to a total acquisition time of 7 h. The powder sample holder was rotated continuously at 15 rpm during data collection to optimize the statistical relevant number of diffracting crystallites and to minimize their possible preferential orientation. Then, the patterns were analyzed with the software package DIFFRAC-PLUS (Bruker) including EVA and TOPAS allowing phase search, single line fitting up to whole powder pattern fitting as well as structure refinement and quantitative analysis by Rietveld method. The details of the analyses are given in the Results section.

Lastly, possible alterations during grinding were assessed by thermogravimetric analyses (TG) performed on raw and ground powders on a Labsys apparatus (SETARAM, France). Experiments were carried out under air using platinum crucibles. Alumina previously fired at 1600 °C is used as the reference material for the mass loss baseline. Powder aliquots of about 200 mg are used. Prior to their analysis, the powders were kept for 48 hours at 100 °C in order to remove ambient absorbed water. Moreover, the heating cycle included a first ramp from room temperature to 100 °C with a dwelling time of 3 h at 100 °C for complete removal of any residual physically adsorbed water. Finally, a heating rate of 5 °C/min was applied from 100 °C to 1000 °C, followed by cooling down to room temperature. The obtained TG data were used to compute the first derivative TG (DTG) with respect to temperature.

3. Results and discussion

3.1. Optimal process parameters

3.1.1. Dry grinding

As shown in Fig. 1 and Table 3, the initial mica powder consists of particles all smaller than 200 μm. The particle size distribution is broad, with a D_{90} of 45 μm and a D_{50} of 12.7 μm. These results are in good agreement with those of the supplier (resp. 20 and 50 μm). According to

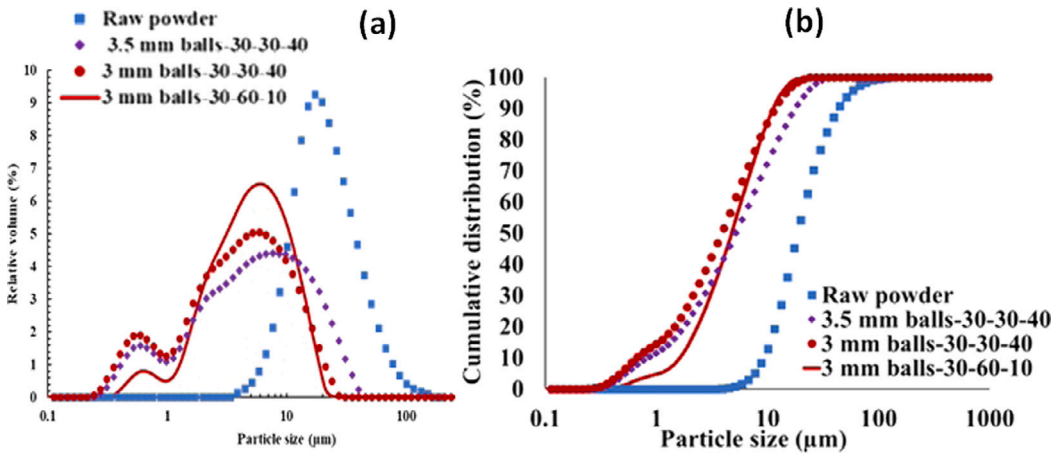

Fig. 1. (a) Typical particle size distributions of dry ground mica powder for different ball sizes and filling proportions. ■: raw powder; ♦: 3.5 mm balls, 30% balls-30% powder-40% air; •: 3 mm balls, 30% balls-30% powder-40% air; solid line: 3 mm balls, 30% balls-60% powder-10% air ; (b) the corresponding cumulative passings.

Table 3
D_{50} and D_{90} at different jar filling rates and ball sizes for dry route. The values before grinding are given for reference. The error bars are standard deviation.

Size	Raw powder	3.5 mm	3 mm	
		30-30-40	30-30-40	30-60-10
D_{50} (µm)	12.7	6	4.4	5.8 ± 0.4
D_{90} (µm)	45	20.3	13.3	14.4 ± 1.6

the observations made with the SEM, these sizes mainly correspond to those of the particles (no agglomerates of size greater than 20 µm, see Fig. 2(a) and (b)). The measured particle density is 2800 ± 2 kg/m^3, which is much smaller than the density of the zirconia grinding balls.

Given the initial particle size distribution of the mica particles and the target size after dry milling (D_{100} smaller than 10 µm and D_{50} around 3 µm), 3 mm and 3.5 mm ball size were tested with a 30-30-40 filling ratio for the dry milling step to achieve effective size reduction according to the recommendations 1–4 of the supplier. Typical particle size distributions obtained after dry milling using different jar filling parameters and grinding ball sizes are shown in Fig. 1. Table 3 shows a summary of the results obtained for D_{50} and D_{90} for all grinding parameters. When several batches were available, average and standard deviation were calculated.

With the chosen 30-30-40 filling, the size of the milling balls had a direct impact on the obtained particle size distribution. As shown in Fig. 1, after only 20 min grinding, with 3 mm balls the particle distribution showed more fine particles than after a grinding with 3.5 mm balls. The D_{90} and D_{50} are respectively equal to 20.3 and 6 µm with 3.5 mm balls and 13.3 and 4.4 µm with the 3 mm balls. It should also be noted that this last value tends towards a theoretical D_{50} a thousand times smaller than the ball size.

Based on these results, 3 mm balls were selected. To determine if it would be possible to increase the amount of recovered ground powder while maintaining a suitable size reduction, the ratio of mica powder in the jar was increased to 60%. In comparison with the 30-30-40 filling, the final particles were a little larger (D_{90} = 14.4 µm and D_{50} = 5.8 µm). This can be due to a lack of free space left (only 10%). Increasing the number of particles increases autogenous grinding because there is more powder and reduces the distances between the particles, decreasing the effect of impact and promoting friction. However, in dry milling and due to the impacts between balls-particles or particles-particles, this closeness leads to the formation of compact agglomerates. However, since the difference with a 30-30-40 configuration is not significant, the 30-60-10 filling with 3 mm balls has been retained as it allows to grind more powder in one go.

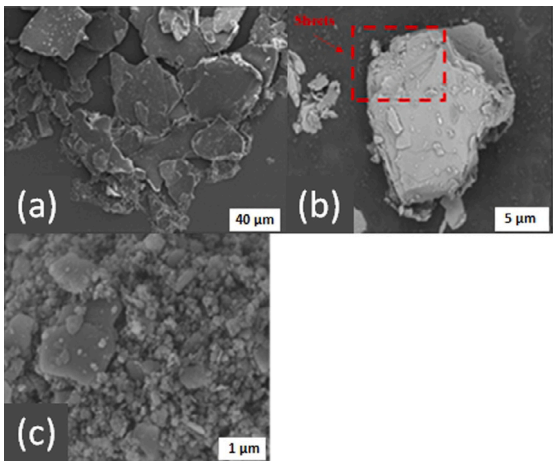

Fig. 2. SEM images of mica particles. (a and b) raw powder ; (c) dry ground powder.

The size reduction was confirmed by the specific surface area measurements. It varied from 5 m^2/g for raw powder to 38 m^2/g after dry grinding using the selected parameters. For all cases, grinding lead to a bi-modal distribution of the particles, with the production of fines (< 1 µm). The images obtained by scanning electron microscopy show that the ground particles are indeed much smaller than 1 µm, suggesting that the entities larger than 1 µm observed in particle size are in fact agglomerates (see Fig. 2(c)).

The target size of the dry milling being obtained, wet milling was performed to reach the size required for inkjet printing.

3.1.2. *Wet grinding*

The dry ground mica powder with an average D_{50} of 5.8 µm was further milled in ethanol using 500 µm balls in order to reach a D_{50} of less than 1 µm. To provide more friction surface as indicated in the recommended rules, a 60-30-10 filling was first tested. With this configuration, the mica particles were reduced to obtain a bimodal particle size distribution with two peaks located around 3 and 0.6 µm (Fig. 3). The value of D_{50} equal to 0.58 µm illustrates the possibility of approaching, with a given ball size (500 µm), particles 1000 times smaller (Table 4).

In order to reduce the quantity of particles or agglomerates above 1 µm, the powder ratio was then reduced to make the mixture less viscous and promote particle motion. With a 60-15-25 filling, although the particle size distribution was still bimodal, the volume of particles

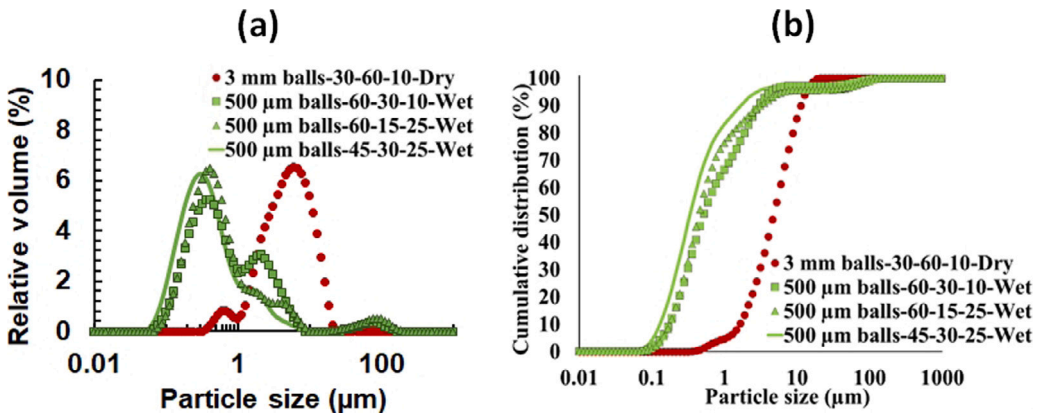

Fig. 3. (a) Evolution of the volumetric particle size distribution of mica powder ground in ethanol with 500 µm balls for 3 different filling proportions. The initial distribution after dry grinding is shown for reference (•). The results for various filling ratios are ■ 60-30-10, ▲ 60-15-25 and solid line 45-30-25. (b) the corresponding cumulative passings.

Table 4
Particle sizes at different jar filling ratios for wet grinding with 500 µm zirconia balls.

Filling ratio	D_{50} (µm)	D_{90} (µm)
60-30-10	0.58	3.4
60-15-25	0.51	4.1
45-30-25	0.38	1.9

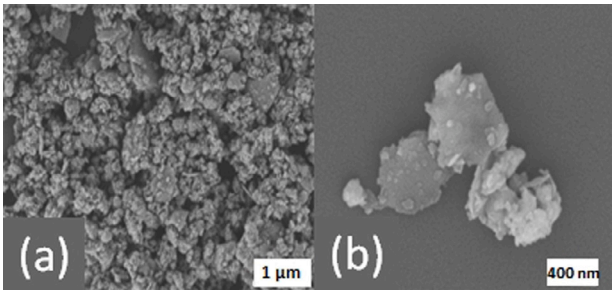

Fig. 4. SEM images of wet ground mica particles at different magnifications.(a) Observation of fine particles ; (b) observation of their shape.

smaller than 10 µm decreased (Fig. 3). In order to increase the powder ratio while keeping a low viscosity, the ratio of balls was reduced to 45% and that of particles increased to 30%, thus increasing autogenous (particle–particle) grinding. With this last configuration 45-30-25, the particle size distribution was shifted towards smaller particle sizes to reach a D_{50} equal to 0.38 µm and a D_{90} of 1.9 µm, which is very close to the target for inkjet printing ink formulation (Table 4, Fig. 3). Based on the images produced by scanning electron microscopy, it should be noted that particles larger than one micron are in fact agglomerates, which it is difficult to avoid during the recovery of the ground material and its laser particle size analysis (Fig. 4). These agglomerates also contribute to the peak around 100 µm observed in the laser granulometry analysis.

Thus, the combination between the use of the Emax, high energy grinder and the adjustment of parameters such as the size of the grinding bodies or the filling ratios lead to a very high fineness of grinding (< 2 µm, > 45 m^2/g).

3.2. Evolution of microstructure and structure of mica

After each grinding step with the optimal size reduction described above, the particle morphology, micro- and crystal structure were monitored to detect possible alterations due to strong energy input during milling. The micrograph in Fig. 2(b) indicates that the initial morphology of the particles is a stacking of sheets typical for phyllosilicate clays. Micrographs in Fig. 2(c) and Fig. 4(b) confirm that the platelet morphology was conserved while the particle size was strongly reduced during the milling steps. The micrograph in Fig. 4(b) also substantiate a wide size distribution going down to nanometric sizes at the end of the milling procedure as observed by laser granulometry. The thickness of the ground platelets still appears very much smaller than the lateral dimension but some agglomerates were observed.

These results indicate that the milling procedure did not produce morphological change while efficiently decreasing the particle size. To check if the minerals suffered structural damage, X-ray diffraction patterns were collected on the samples. All patterns are shown in Fig. 5.

The raw mica diffractogram shows sharp reflections which were assigned to the three expected mineral phases with a high degree of crystallinity, namely muscovite ($KAl_3Si_3O_{12}H_2$, JCPDS 010820576), kaolinite ($Al_2Si_2O_9H_4$, JCPDS 040133074) and quartz (SiO_2, JCPDS 000461045). The very few remaining humps with extremely weak intensities did not allow identifying potassium feldspar ($KAlSi_3O_8$), as it is expected to be present in too small quantities. The platelet shape of the particles observed on SEM micrographs induces an unavoidable preferred orientation whatever the method of preparation of the diffraction sample, resulting in an increase of the intensities of (00l) muscovite reflections (c-direction), and to a lesser degree those of kaolinite.

Taking into account the X-ray beam geometry, the diffractometer characteristics and starting from the crystallographic structure extracted from the ICDD-JCPDS database for each mineral component, Rietveld quantitative phase analysis [34] was performed to calculate their weight fractions using the program TOPAS. To improve the refinement, the (00l) preferred orientation was assumed for muscovite as well as for kaolinite and only their lattice and peak-broadening parameters were refined. The cation occupancies in the octahedral and tetrahedral sheets were kept fixed during the quantification. As quartz has few visible peaks with low intensity, its parameters were also kept fixed at a given refinement step and were manually adjusted if needed between two refinement steps using isolated lines such as (010) and (112) and knowing that a=b. As non-structural parameters, the zero and sample displacement errors and a Chebychev polynomial of 4th degree for background modeling were also refined. The weight fraction of the different mineral phases obtained after following this procedure were 81.1, 13.7 and 5.3 wt % of muscovite, kaolinite and quartz respectively, in good agreement with the supplier's data. The preferential orientation obtained from the refinement was respectively 0.75 and 0.78 for muscovite and kaolinite in the raw powder.

Upon grinding, the characteristic peaks of the different mica phases were still detected and no new peak arose which confirms that the mica powder has not undergone polymorphic transformation during grinding and hence no new phase appeared. However, the sharp reflections of

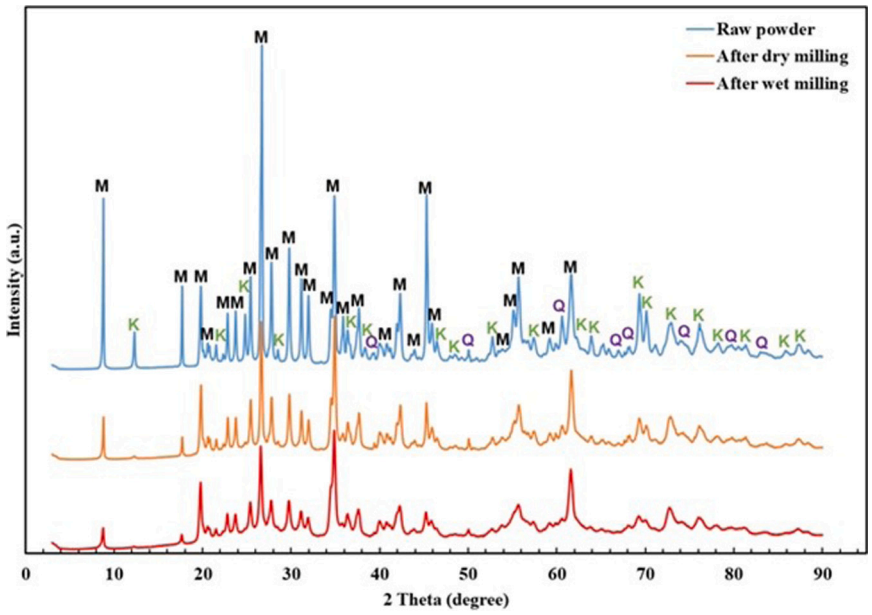

Fig. 5. X-ray patterns of raw mica powder and after each grinding step. From bottom to top, blue: raw mica, orange: dry ground and red: ethanol ground with dispersant. The curves are shifted vertically for clarity. The peaks of the different minerals (muscovite, kaolinite and quartz, resp. JCPDS 010820576, 040133074 and 000461045) are indexed on the raw powder pattern.

the raw mica gradually weakened in intensity and broadened after the dry as well as the wet comminution while the background scattering increased. Grinding caused a rapid decrease in the relative peak area of the (00l) reflections of both muscovite and kaolinite while the decrease in intensity of the other peaks was different depending on Miller's indices, probably reflecting the differences in mechanical properties in the a, b and c directions. The main loss of the (00l) peak area was observed after the dry stage of grinding while the reduction was weaker after the wet stage. In the case of phyllosilicates (layered minerals) such as muscovite as well as kaolinite a decrease in particle size is achieved by: (1) delamination by cleavage along the basal planes, or (2) fragmentation of particles according to the surface perpendicular to the basal plane, which leads to the creation of new lateral surfaces [35]. Although a part of the (00l) peak area decrease was due to the lowering of preferred orientation which is no more observable for ground samples (see below), dry grinding seems to significantly favor the delamination process as the relative peak areas of the (00l) reflections were drastically diminished as expected from the thinning of the muscovite and kaolinite plates.

After wet grinding, only the (001) kaolinite reflection was present in the form of a very weak intensity broad peak centered around 12.4° in 2θ as previously observed in the literature [36]. Thus, the X-ray patterns suggest that the kaolinite suffered the largest microstructural and structural alterations while the harder quartz grains of the raw mica powder suffered the least as no detectable changes in the reflections of the quartz were found except line broadening. This result agrees with the Mohs hardness value of each mineral phase, which is 2, between 2.8 and 3.2 and 7 for kaolinite, muscovite and quartz respectively. As mentioned by Makó et al. it could be noted that the quartz grains could act as additional grinding bodies [36].

The background scattering increase after milling, supported by the occurrence of an 'amorphous hump', as seen in Fig. 5 in the 20–35° region and associated with the peak intensity decrease, is generally interpreted by the amorphization of the minerals due to the partial destruction of their structure by distortion and breakage of their crystalline network as well as by the formation of internal defects [37]. The chemical composition of this amorphous phase is unknown. We can also argue that the creation of nanocrystals during milling will also lead to peak broadening and the occurrence of humps on XRD patterns resembling an amorphous material [38]. The X-ray diffraction alone cannot decide between these two hypotheses, i.e. amorphization or diffracting nanocrystals.

The analysis of the muscovite relative crystallinity based on the XRD pattern data by using, for example, the intensity of the strongest characteristic peaks [37], i.e., by simply dividing the intensity of the (006) comminuted muscovite reflection by the intensity of the same peak in raw muscovite is questionable. Indeed, the absolute intensity of a given peak can vary due to instrumental and experimental parameters such as unavoidable preferred orientation for platelet crystals during sample preparation. Moreover, such a preferred orientation varies with the platelet size, which decreases during grinding.

Rietveld quantitative phase analysis was also performed on dry and wet comminuted mica powders. As the only detectable remaining peak for kaolinite was the (001), only the c cell parameter and those related to the variation of kaolinite peak-broadening as a function of 2θ can be refined. The amorphization and/or crystal nanosizing was considered by adding a broad peak in the 20–35° range [17]. The refinement procedure was adapted accordingly, the quartz cell parameters being controlled and slightly adjusted throughout the refinement as before. The whole pattern fitting showed that the preferred orientation due to sample preparation was no more observable (0.98 for muscovite and already 1 for kaolinite after the dry stage, 1 for all minerals after dry grinding) and was subsequently removed from the refinement. It seems coherent with particle morphology seen on SEM micrographs where the aspect ratio between side and edge dimensions, whose high value favors orientation, decreases. According to the symmetric or asymmetric shape of the inserted 'amorphous hump', the degree of crystallinity of mica powders was evaluated between 80%–90% and 70%–83% for dry and wet grinding respectively. Moreover, the computed ratio of kaolinite was clearly reduced.

To sum up the results of the Rietveld procedure, the refined cell parameters a, b and c for muscovite remained strictly constant as well as the adjusted a and c parameters for quartz. Even though a decrease in the intensity of the diffracting peaks was observed, substantial changes in the structure were not detected by X-ray diffraction. It indicates that the mechanical forces applied in the grinding procedure were not strong enough to induce distortions in the crystal structure. For a more exact representation of the microstructural change through diffraction

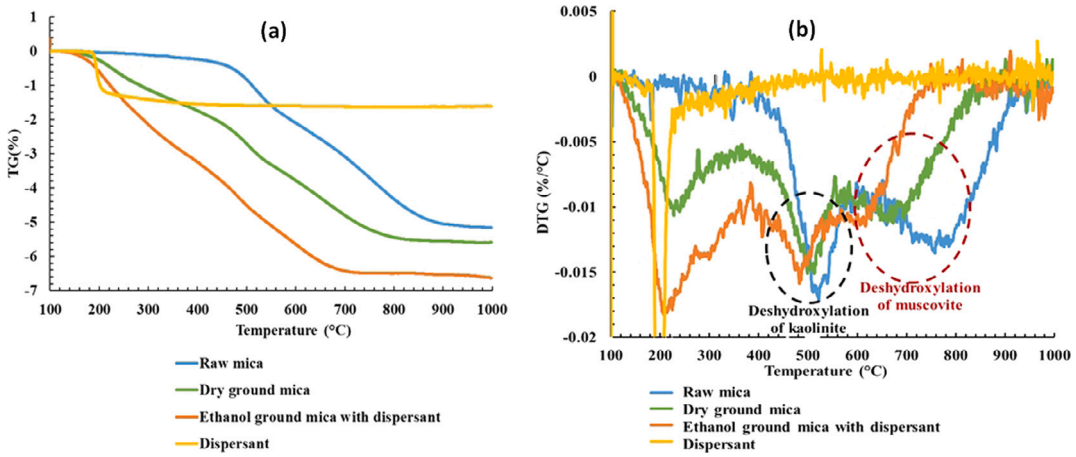

Fig. 6. TG (a) and DTG (b) curves for. raw mica (blue line); dry ground mica (green line); ethanol ground mica with dispersant (orange line) and dispersant (yellow line). Dehydroxylation of kaolinite and muscovite occur at high temperature, appearing as negative peaks in the DTG curve.

data, the full widths at half maximum (FWHM) of the main isolated diffraction peaks of each mineral were calculated. As a general trend, a significant increase of the FWHM was observed after the wet stage of grinding while there was a smaller one after the dry stage. The shape and broadening of the XRD line profiles may be connected to crystallite size and/or to mean lattice strain [38] as well as to stacking faults which could also be largely present in such natural minerals [39] or to any other lattice imperfection or defect.

Thus, X-ray diffraction confirmed the unaltered muscovite structure of the ground materials. A large part of the micrometric and submicron particles obtained thereby retained the plate-like shape and the crystalline structure of the muscovite mineral.

To confirm these results, thermogravimetric analyses were performed on the raw powder and after the milling steps in order to quantify the mass loss related to expected reactions occurring in muscovite and kaolinite. The results for mass variation as a function of temperature for all samples are shown in Fig. 6.

In agreement with [30], the first peak of the DTG curve of raw mica located between 400 and 600 °C associated with a mass loss of 2.1% was attributed to the elimination of water of structural origin corresponding to the dehydroxylation of kaolinite by a diffusional mechanism [40] leading to the formation of metakaolinite (amorphous phase).

The position and shape (height and width) of dehydroxylation peaks are sensitive to the particle size [16,41]. Indeed, this peak tends to be shifted to lower temperatures when the particle size is decreased, due to the increase of the surface area. The reaction kinetics is also faster. The DTG peak shifts were significantly larger for muscovite than for kaolinite. This trend could be explained by muscovite particles being initially larger than kaolinite. Also, the dehydroxylation peak of muscovite overlapped with the peak of kaolinite upon grinding, which made quantitative analysis impossible.

The additional mass loss observed at temperatures between 100 and 400 °C on the DTG curves of wet ground mica cannot be attributed only to the removal of dispersant adsorbed on the particle surface because it was also present for dry ground mica without dispersant. TG and DTG curves of dispersant alone indicate that it burns at temperatures between 150 and 250 °C. This additional peak can be attributed to the removal of interlayer water, absorbed between sheets of mica after grinding. The increase in the specific surface area after grinding makes the particles highly reactive towards water present in the ambient air. For the wet ground case, that new surface area could also be occupied by the dispersant.

4. Conclusion

The objective of this study was to grind a commercial mica powder in order to make it compatible with the inkjet process which requires particle sizes below 1 μm in the most efficient way using a high energy ball mill. Grinding required two steps: a dry grinding which reduced the particle size from 45 μm down to 15 μm and a wet step in ethanol reaching a particle size of 2 μm. The optimal jar filling ratios and ball size for each step were 3 mm balls and 30-60-10 for dry and 500 μm with 45-30-25 for the wet step. It appears that autogenous grinding was favorable for the case of dry grinding (high powder ratio) whereas more solvent was needed for the wet step to be efficient. The final results are satisfying regarding the size requirements and considering that mica is a very difficult material to grind due to its softness. Morphological and structural characterizations during the milling process indicated no phase change in the composition of the mica powder (muscovite, kaolinite and quartz). The effects of size reduction were seen in the shift towards lower temperatures of dehydroxylation peaks for mica and muscovite due to the increase in specific surface area, as well as in the broadening of X-ray diffraction peaks and in the reduction of preferential orientation. So, no numerical values of size as well as strain could be reasonably given. Qualitatively, the line broadening increase illustrated the crystallite size decrease, which was more efficient during wet grinding, and the kaolinite crystals were smaller than those of muscovite (assuming constant strain).

In conclusion, an efficient grinding protocol of a raw commercial mica was successfully worked out to obtain a micrometric grain size powder. Moreover, the morphology and crystallographic structure were unchanged so it is expected that the physico-chemical properties of the raw mica have also been preserved. This paves the way for the formulation of organic inks to elaborate components by inkjet printing.

CRediT authorship contribution statement

Naima Boughazif: Formal analysis, Writing – original draft, Writing – review & editing, Investigation. **Fabien Gerschwitz:** Investigation. **Julie Bourret:** Formal analysis, Investigation, Writing – original draft, Writing – review & editing. **Gisèle Lecomte-Nana:** Formal analysis. **André Lecomte:** Formal analysis, Investigation, Writing – original draft. **Martine Lejeune:** Formal analysis, Supervision, Writing – original draft. **Vincent Rat:** Formal analysis, Supervision, Writing – original draft. **Marguerite Bienia:** Formal analysis Investigation, Supervision, Writing – original draft, Writing – review & editing.

Declaration of competing interest

The authors declare that they have no known competing financial interests or personal relationships that could have appeared to influence the work reported in this paper.

Data availability

The data that has been used is confidential.

Acknowledgments

This project benefited from a regional Nouvelle-Aquitaine grant for doctoral thesis (N. Boughazif) and equipment RNA19431 C431.

References

[1] A.S. Gray, C. Uher, Thermal conductivity of mica at low temperatures, J. Mater. Sci. 12 (5) (1977) 959–965.
[2] A. Anton, J.L. Steinle, Micas et produits micacés, Tech. l'ingénieur (1997) 25.
[3] R.J. Benbow, B.H.W.S. De Jong, J.W. Adams, Mica, ISBN: 978-3-527-30673-2, 2000, p. a16_551, http://dx.doi.org/10.1002/14356007.a16_551.
[4] S.G. Barlow, D.A.C. Manning, Influence of time and temperature on reactions and transformations of muscovite mica, Br. Ceram. Trans. 98 (3) (1999) 122–126.
[5] K. Sztymela, M. Bienia, F. Rossignol, S. Mailley, S. Ziesche, J. Varghese, M. Cerbelaud, Fabrication of modern lithium ion batteries by 3D inkjet printing: opportunities and challenges, Heliyon (2022).
[6] M. Lejeune, T. Chartier, C. Dossou-Yovo, R. Noguera, Ink-jet printing of ceramic micro-pillar arrays, J. Eur. Ceram. Soc. 29 (5) (2009) 905–911.
[7] Y.S. Kim, W. Chang, H.J. Jeong, K.H. Kim, H.S. Park, J.H. Shim, High performance of protonic ceramic fuel cells with 1-μm-thick electrolytes fabricated by inkjet printing, Addit. Manuf. 71 (2023).
[8] W. Chang, E.H. Kang, H.J. Jeong, W. Choi, J.H. Shim, Inkjet printing of perovskite ceramics for high-performance proton ceramic fuel cells, Energy 268 (2023).
[9] H. Li, H. Zhang, F. Li, A. Chang, H. Zhuo, Ink-jet printed new core@shell ceramic for high stability NTC thermistors, Ceram. Int. 49 (12) (2023) 20832–20838.
[10] C. Liang, J. Huang, J. Wang, H. Gong, W. Guo, R. Cao, P. Zhao, Three-dimensional inkjet printing and low temperature sintering of silica-based ceramics, J. Eur. Ceram. Soc. 43 (5) (2023) 2289–2294.
[11] S.F. Santos, S.C.A. França, T. Ogasawara, Method for grinding and delaminating muscovite, Min. Sci. Technol. (China) 21 (1) (2011) 7–10.
[12] L. Andrić, A. Terzić, Z. Aćimović-Pavlović, M. Trumić, M. Petrov, L. Pavlović, A kinetic study of micronization grinding of dry mica in a planetary ball mill, Adv. Mater. Sci. Eng. 2013 (2013) 1–6.
[13] Retsch GmbH Webinar, Useful tips for efficient grinding in laboratory ball mills, 2023.
[14] L.A. Pérez-Maqueda, F. Franco, M.A. Avilés, J. Poyato, J.L. Pérez-Rodríguez, Effect of sonication on particle-size distribution in natural muscovite and biotite, Clays Clay Miner. 51 (6) (2003) 701–708.
[15] E. Papirer, P. Roland, M. Nardin, H. Balard, Variation of the surface energy characteristics of mica (muscovite) upon grinding, J. Colloid Interface Sci. 113 (1) (1986) 62–66.
[16] R. Mackenzie, The effect of grinding on micas. I. Muscovite, Clay Miner. 30 (222) (1953) 178–185.
[17] R. Grèzes-Besset, M. Mouysset-Espagne, Sur les conditions de libération d'eau et de fluor par les micas soumis à des actions mécaniques et thermiques, Bull. Minéralogie 103 (6) (1980) 591–595.
[18] O. Trass, E.A.J. Gandolfi, Fine grinding of mica in the Szego Mill, Powder Technol. 60 (3) (1990) 273–279.
[19] E. Papirer, A. Eckhardt, F. Muller, J. Yvon, Grinding of muscovite: influence of the grinding medium, J. Mater. Sci. 25 (12) (1990) 5109–5117.
[20] E. Papirer, P. Martz, Ball milling of muscovite in organic media, Mater. Sci. Eng. 95 (C) (1987) L5.
[21] J. Yvon, J.M. Cases, P.H. De Donato, M. Kongolo, L. Michot, Conséquences superficielles et structurales de la fragmentation mécanique mines et carrières : Les techniques-broyage III-IV, (18) 1996.
[22] J.-l. Dandurand, Contribution à l'étude des effets du broyage sur les transformations physico-chimiques des minéraux (Ph.D. thesis), 1978.
[23] G. Suraj, C.S.P. Iyer, S. Rugmini, M. Lalithambika, The effect of micronization on kaolinites and their sorption behaviour, Appl. Clay Sci. 12 (1–2) (1997) 111–130.
[24] G. Baudet, V. Perrotel, A. Seron, M. Stellatelli, Two dimensions comminution of kaolinite clay particles, in: Powder Technology, vol. 105, Elsevier Sequoia SA, pp. 125–134.
[25] P.J. Sánchez-Soto, M. Del Carmen Jiménez De Haro, L.A. Pérez-Maqueda, I. Varona, J.L. Pérez-Rodríguez, Effects of dry grinding on the structural changes of kaolinite powders, J. Am. Ceram. Soc. 83 (7) (2000) 1649–1657.
[26] F. Dellisanti, G. Valdré, Study of structural properties of ion treated and mechanically deformed commercial bentonite, Appl. Clay Sci. 28 (1-4 SPEC. ISS.) (2005) 233–244.
[27] J. Hrachová, J. Madejová, P. Billik, P. Komadel, V.S. Fajnor, Dry grinding of Ca and octadecyltrimethylammonium montmorillonite, J. Colloid Interface Sci. 316 (2) (2007) 589–595.
[28] N. Vdović, I. Jurina, S.D. Škapin, I. Sondi, The surface properties of clay minerals modified by intensive dry milling — revisited, Appl. Clay Sci. 48 (4) (2010) 575–580.
[29] K. Klier, A.C. Zettlemoyer, Water at interfaces: Molecular structure and dynamics, J. Colloid Interface Sci. 58 (2) (1977) 216–229.
[30] F. Gridi-Bennadji, Matériaux de mullite à microstructure organisée composés d'assemblages muscovite - kaolinite (Ph.D. thesis), 2007.
[31] C.F. Burmeister, M. Hofer, P. Molaiyan, P. Michalowski, A. Kwade, Characterization of stressing conditions in a high energy ball mill by discrete element simulations, Processes 10 (4) (2022).
[32] Retsch GmbH, The art of milling, 2017.
[33] R.E. Schilling, Choose the right grinding mill, Chem. Process. 73 (10) (2010) 33–38.
[34] K. Ufer, H. Stanjek, G. Roth, R. Dohrmann, R. Kleeberg, S. Kaufhold, Quantitative phase analysis of bentonites by the Rietveld method, Clays Clay Miner. 56 (2) (2008) 272–282.
[35] H. Balard, O. Aouadj, E. Papirer, Monitoring, by inverse gas chromatography, of the variation of the surface energetic heterogeneity of ground muscovite samples, Langmuir 13 (5) (1997) 1251–1255.
[36] É. Makó, R.L. Frost, J. Kristóf, E. Horváth, The effect of quartz content on the mechanochemical activation of kaolinite, J. Colloid Interface Sci. 244 (2) (2001) 359–364.
[37] G. Yao, H. Zang, J. Wang, P. Wu, J. Qiu, X. Lyu, Effect of mechanical activation on the pozzolanic activity of muscovite, Clays Clay Miner. 67 (3) (2019) 209–216.
[38] D. Balzar, X-ray diffraction line broadening: modeling and applications to high-Tc superconductors, J. Res. Natl. Inst. Stand. Technol. 98 (3) (1993) 321.
[39] G.W. Brindley, G. Brun, Crystal structures of clay minerals and their X-Ray identification, 1980, http://dx.doi.org/10.1180/mono-5.
[40] E. Gámiz, M. Melgosa, M. Sánchez-Marañón, J.M. Martín-García, R. Delgado, Relationships between chemico-mineralogical composition and color properties in selected natural and calcined Spanish kaolins, Appl. Clay Sci. 28 (1–4) (2005) 269–282.
[41] L.A. Pérez-Maqueda, J.M. Blanes, J. Pascual, J.L. Pérez-Rodríguez, The influence of sonication on the thermal behavior of muscovite and biotite, J. Eur. Ceram. Soc. 24 (9) (2004) 2793–2801.